Track-Following Control with Active Vibration Damping of a PZT-Actuated Suspension Dual-Stage Servo System *

Yunfeng Li[†], Federico Marcassa[‡], Roberto Horowitz[†], Roberto Oboe[‡], and Robert Evans[§]

[†] Dept. of Mechanical Engineering, University of California at Berkeley, CA 94720-1740, USA

[‡]Dept. of Information Engineering, University of Padova, PD, 35131, ITALY

[§]Hutchinson Technology Incorporated, Hutchinson, MN 55350, USA

Abstract

This paper discusses the controller design of a PZT-actuated suspension dual-stage servo system in hard disk drives. The proposed control structure includes an active vibration damping control loop and a track-following control loop. The vibration damping control loop, which runs at a faster rate than the track-following control loop, utilizes a PZT element on a PZT-actuated suspension as a vibration sensor to damp the resonance modes of the voice coil motor (VCM) and the PZT actuator. The vibration damping controller is designed using Kalman filter based state feedback control techniques. A simple dual-stage track-following controller is designed, based on the damped actuator model, using the sensitivity function decoupling design method. Simulation and experimental results are presented to demonstrate the benefits of this control scheme in expanding servo control bandwidth and suppressing airflow excited structural vibrations.

1 Introduction

The use of a PZT-actuated suspensions as a second stage actuator has been proposed as one approach to dual-stage actuation in hard disk drives [1]. Compared to the actuated slider/head approach, the main disadvantage of this approach is that the PZT actuator is located between the E-block arm and the suspension, and can excite their vibration modes. Normally notch filters are utilized in disk drive servo control designs

*Research supported by the National Storage Industry Consortium (NSIC) and the Computer Mechanics Laboratory (CML) of U.C. Berkeley. Corresponding author E-mail: horowitz@me.berkeley.edu

to ensure the stability of the control system. However, notch filters reduce phase margin and detrimentally affect the controller robustness [2], [3].

Furthermore, the arm and suspension vibration modes can be excited by the airflow generated from disk rotation, which causes undesirable head off-track motion. Airflow excited vibration (windage) is one of the major position error sources for high-RPM disk drives. In order to generate large motion range and reduce driving voltage, PZT-actuated suspensions are usually designed to have a relatively low frequency in-plane sway mode. This makes them to be more susceptible to airflow excitations than conventional suspensions.

A controller designed using notch filters cannot attenuate the windage effect on the structural vibration modes [3]. Moreover, because most of these vibration modes have resonance frequencies that are higher than the servo bandwidth, the windage-induced vibrations are often amplified by the closed-loop servo system. In [3], a phase-stabilized servo controller has been designed to suppress the track-mis-registration (TMR) due to airflow excited structural vibrations. Active vibration control is another approach to increase servo bandwidth and suppress vibration induced TMR [2],[4].

Because the sampling frequency of the position error signal (PES) is limited by the data storage efficiency, additional vibration sensors are usually needed to implement active vibration control. For a PZT-actuated suspension, one of the two PZT elements can be utilized as a vibration sensor to damp the head stack and suspension assembly vibration modes [4]. In this paper, a track-following control design combined with this vibration damping control scheme is presented. A new state feedback damping controller has been designed based on Kalman filter modal estimation. A simple track-following controller is designed using a sensitivity function decoupling method [6]. Notch filters are not used in the track-following control design because the vibration modes are adequately damped.

Section 2 describes the modeling of the control system. Section 3 discusses the damping controller and track-following controller designs. Section 4 presents the experimental results obtained with a hard disk drive (HDD) controlled using an external DSP and a Laser Doppler Vibrometer (LDV), which confirm the efficacy of the proposed control scheme in suppressing structural vibrations and enhancing the overall performance of the servo system. Section 5 concludes the paper.

2 Sensor and Actuator Modeling

2.1 Frequency Response Modal Testing

The considered plant is a two-input two-output control system. Let u_1 and u_2 be the input to the voice coil motor (VCM) and the PZT actuator respectively, and y_1 and y_2 be the head displacement output in the

radial off-track direction and the PZT vibration sensor output respectively. The transfer function from u_j to y_i, $G_{ij}(s)$, $i, j = 1, 2$, can be written as

$$G_{ij}(s) = \frac{K_0^{ij}}{s^2} + \sum_{n=1}^{N} \frac{\omega_n^2 K_n^{ij}}{s^2 + 2\zeta_n \omega_n s + \omega_n^2} + d_{ij}, \tag{1}$$

which is the summation of the rigid body mode, a number of structural vibration modes and a direct feeding term from the input to the output. In Eq. (1), K_0^{ij} is the gain of the rigid body mode, N is the total number of vibration modes being considered, ω_n and ζ_n are the natural frequency and the damping ratio of mode n respectively, K_n^{ij} is the modal constant of mode n from u_j to y_i, and d_{ij} is the direct feed through factor from u_j to y_i.

Figs. 1-4 show the following measured and simulated frequency responses: a) from VCM input u_1 to head displacement y_1; b) from PZT actuator input u_2 to head displacement y_1; c) from VCM input u_1 to PZT sensor output y_2; d) from PZT actuator input u_2 to PZT sensor output y_2. The solid lines are experimentally measured responses, while the dashed lines are simulated responses using the identified model.

As shown in these figures, major vibration modes of the PZT-actuated suspension dual-stage actuator in our setup include the assembly butterfly mode (M1 in the figures), the suspension sway mode (M2), the suspension 2nd torsion mode (M3), and the suspension 1st torsion mode (M4). Among them, the two most important off-track modes are the assembly butterfly mode and the suspension sway mode. Fig. 5 illustrates the mode shapes of these two modes. The assembly butterfly mode is generated by the coupling of in-plane sway modes of the E-block arm and the coil, in which the arm and the coil move out of the phase with respect to each other around the pivot. The suspension sway mode is the vibration of the load beam and the slider with respect to the hinge of the PZT-actuated suspension. It is also called the PZT actuator mode.

As shown in Fig. 1, the frequency response from VCM input u_1 to head displacement y_1 is dominated by the rigid body mode in the low frequency range and the structural vibration modes in the high frequency range. Fig. 2 shows that the PZT actuator can excite the VCM actuator butterfly mode through the swage connection with the E-block arm.

As shown in Figs. 3-4, the PZT sensor can pick up most of the off-track vibration modes of the head stack and suspension assembly when they are excited by the control inputs. The PZT sensor does not sense the rigid body mode, as expected. However, the PZT sensor picks up some non-off-track modes near 3 kHz (M5 and M6 in Figs. 3-4), which have little effect on the head off-track motion. These modes are probably related to the bending modes of the suspension and they are excited by the airflow disturbances in the out-of-the-plane direction. They act as noise modes to the control system.

2.2 State Space Model Realization

The control system model can be represented using a state space model based on the transfer functions in Eq. (1) and the extracted modal parameters. The rigid body mode is not observable from the PZT sensor output, and hence not included in the state space model for vibration damping control design. A state space realization including the three vibration modes M1, M2, and M3 is:

$$\begin{aligned} \dot{\mathbf{x}} &= \mathbf{A}\mathbf{x} + \mathbf{B}\mathbf{u}\,, \\ \mathbf{y} &= \mathbf{C}\mathbf{x} + \mathbf{D}\mathbf{u}\,, \end{aligned} \tag{2}$$

where $\mathbf{x} = [x_1\, x_2\, x_3\, x_4\, x_5\, x_6]^T$, $\mathbf{u} = [u_1\, u_2]^T$, $\mathbf{y} = [y_1\, y_2]^T$. u_1 and u_2 represent the inputs to the VCM and the PZT actuator, respectively. y_1 and y_2 represent the head displacement output (excluding the rigid body mode) and the PZT sensor output, respectively. The decoupled state matrices can be written as

$$\begin{aligned} \mathbf{A} &= \begin{bmatrix} A_1 & 0_{2\times2} & 0_{2\times2} \\ 0_{2\times2} & A_2 & 0_{2\times2} \\ 0_{2\times2} & 0_{2\times2} & A_3 \end{bmatrix}, \qquad \mathbf{B} = \begin{bmatrix} B_1 \\ B_2 \\ B_3 \end{bmatrix}, \\ \mathbf{C} &= \begin{bmatrix} c_{11} & 0 & c_{12} & 0 & c_{13} & 0 \\ c_{21} & 0 & c_{22} & 0 & c_{23} & 0 \end{bmatrix}, \quad \mathbf{D} = \begin{bmatrix} 0_{1\times2} \\ D_2 \end{bmatrix}, \end{aligned} \tag{3}$$

where each sub-matrix is expressed as

$$\begin{aligned} A_n &= \begin{bmatrix} 0 & 1 \\ a_{n1} & a_{n2} \end{bmatrix}, \quad B_n = \begin{bmatrix} 0 & 0 \\ b_{n1} & b_{n2} \end{bmatrix}, \\ n &= 1, 2, 3. \end{aligned} \tag{4}$$

where

$$a_{n1} = -\omega_n^2, \quad a_{n2} = -2\zeta_n\omega_n\,, \tag{5}$$

and by normalizing the PZT sensor output equation with $c_{2n} = 1, n = 1, 2, 3$, we have

$$\begin{aligned} b_{n1} &= K_n^{21}, \quad b_{n2} = K_n^{22}\,, \\ c_{1n} &= K_n^{11}/K_n^{21} = K_n^{12}/K_n^{22}\,. \end{aligned} \tag{6}$$

2.3 Airflow Excited Vibrations

Fig. 6 shows the power spectral densities (PSD) of the head off-track motion (upper half) and the PZT sensor output (lower half) when the spindle is rotating in a 7200-RPM disk drive and no control action is applied.

As shown in the figure, the major off-track modes excited by air turbulence generated by disk rotation include the butterfly mode (M1), and the suspension sway mode (M2), the suspension 1st and 2nd torsion mode (M4 and M3). The PZT sensor is able to sense the vibrations of modes M2 and M3 when they are excited by airflow disturbances, but not M1 and M4. Modes M5, M6, and M7 have a large contribution to the PZT sensor output, yet they have little contribution to the head off-track motion. These modes are probably related to the bending modes of the suspension in the out-of-the-plane direction. They will be modeled as sensor noise modes in the Kalman filter design.

3 Controller Design

The proposed overall control structure, which includes a vibration damping control loop and a track-following control loop, is based on the block diagram shown in Fig. 7. P represents the augmented plant model, which will be described in section 3.1.1, and $\mathbf{w}$ represents the airflow disturbances acting on the system. The damping controller is implemented using the PZT sensor output y_2, so that its sampling frequency will not be limited by that of the PES. A inner-loop vibration damping controller is designed first. Then, the outer-loop track-following controller is designed based on the damped actuator model.

3.1 Damping Control Design

In [4], a vibration damping controller was designed using the H_∞ control design method, in which weighting functions were used to characterize disturbance, noise and control design objectives. In order to have a better characterization of the sensor noise and to directly account for the computational time delay effect, a new damping control design method based on Kalman filter and state feedback control is proposed. An augmented plant model with disturbance and sensor noise modes has been used to design the Kalman filter for model estimation. The state feedback damping controller has been designed using the discrete-time-linear-quadratic-regulator (DLQR) method.

3.1.1 Augmented Plant Model for Kalman Filter Design

As shown in Fig. 6, modes M5, M6, and M7 have a large contribution to the PZT sensor output when excited by airflow disturbances, but have little contribution to the head off-track motion. Moreover, they are either not controllable or weakly controllable by the control inputs. Thus, they will be modeled as sensor noise and will be accounted for in an augmented plant model described by

$$\begin{aligned}
\begin{bmatrix} \dot{\mathbf{x}} \\ \dot{\mathbf{x}}_{\mathbf{w}} \end{bmatrix} &= \begin{bmatrix} \mathbf{A} & \mathbf{0} \\ \mathbf{0} & \mathbf{A_w} \end{bmatrix} \begin{bmatrix} \mathbf{x} \\ \mathbf{x_w} \end{bmatrix} + \begin{bmatrix} \mathbf{B} & \mathbf{B_w 1} \\ \mathbf{0} & \mathbf{B_w 2} \end{bmatrix} \begin{bmatrix} \mathbf{u} \\ \mathbf{w} \end{bmatrix}, \\
\begin{bmatrix} \mathbf{y_1} \\ \mathbf{y_2} \end{bmatrix} &= \begin{bmatrix} \mathbf{C_1} & \mathbf{0} \\ \mathbf{C_2} & \mathbf{C_w} \end{bmatrix} \begin{bmatrix} \mathbf{x} \\ \mathbf{x_w} \end{bmatrix} + \begin{bmatrix} \mathbf{D} & \mathbf{0} \end{bmatrix} \begin{bmatrix} \mathbf{u} \\ \mathbf{w} \end{bmatrix},
\end{aligned} \tag{7}$$

where $\mathbf{x} \in \mathbb{R}^6$ represents the state of the three vibration modes to be controlled (M1, M2, M3); $\mathbf{A}$, $\mathbf{B}$, $\mathbf{C_1}$, and $\mathbf{C_2}$ are given by Eqs. (2)-(6); $\mathbf{x_w} \in \mathbb{R}^6$ represents the state variables of the three noise modes (M5, M6, M7); $\mathbf{w} \in \mathbb{R}^6$ is a fictitious white disturbance vector used to characterize the excitation to each vibration mode by airflow disturbances; $\mathbf{A_w}$ is estimated from the measured PSD in Fig. 6; $\mathbf{B_w}$ and $\mathbf{C_w}$ are normalized.

The discrete-time model of P in Eq. (7), with computational-time delay t_d, can be written as follows [5]

$$\begin{aligned}
\begin{bmatrix} \mathbf{x}(k+1) \\ \mathbf{x_w}(k+1) \\ \mathbf{u}(k) \end{bmatrix} &= \begin{bmatrix} \mathbf{\Phi} & 0 & \mathbf{\Gamma_1} \\ 0 & \mathbf{\Phi_w} & 0 \\ 0 & 0 & 0 \end{bmatrix} \begin{bmatrix} \mathbf{x}(k) \\ \mathbf{x_w}(k) \\ \mathbf{u}(k-1) \end{bmatrix} + \\
&\quad + \begin{bmatrix} \mathbf{\Gamma_2} \\ 0 \\ I \end{bmatrix} \mathbf{u}(k) + \begin{bmatrix} \mathbf{\Gamma_w} \end{bmatrix} \mathbf{w}(k), \qquad . \\
\begin{bmatrix} \mathbf{y_1}(k) \\ \mathbf{y_2}(k) \end{bmatrix} &= \begin{bmatrix} \mathbf{C} & \mathbf{C_w} & \mathbf{D} \end{bmatrix} \begin{bmatrix} \mathbf{x}(k) \\ \mathbf{x_w}(k) \\ \mathbf{u}(k-1) \end{bmatrix}
\end{aligned} \tag{8}$$

Assuming the computational time delay t_d is smaller than the sampling time T_s, we have

$$\Phi = e^{AT_s}\,, \tag{9}$$

$$\Phi_w = e^{A_w T_s}\,, \tag{10}$$

$$\Gamma_1 = \int_0^{t_d} e^{A\tau} B d\tau\,, \tag{11}$$

$$\Gamma_2 = \int_{t_d}^{T_s} e^{A\tau} B d\tau\,, \tag{12}$$

$$\Gamma_w = \int_0^{T_s} e^{A_w \tau} B_w d\tau\,. \tag{13}$$

3.1.2 Kalman filter and DLQR design

A discrete-time Kalman filter with prediction and correction steps was designed based on the augmented discrete-time plant model defined in Eq. (8), to estimate the state of the vibration modes. The two design parameters of the Kalman filter are the covariance matrix $\mathbf{W}$ of the disturbance vector $\mathbf{w}$ and the noise variance V_2 of the PZT sensor output y_2. The disturbance covariance matrix $\mathbf{W}$ can be estimated from the PSD of the PZT sensor output (see Fig. 6), since the disturbance input matrix $\mathbf{B_w}$ and the output matrix $\mathbf{C_w}$ are normalized. The measurement noise variance V_2 can be tuned as a design parameter to set the bandwidth of the observer.

The design of the feedback gain matrix was based on the discretization with computational delay t_d of the control plant model defined in Eq. (2). The feedback damping controller gain $\mathbf{K}$ was generated by a DLQR which minimizes

$$\sum_k \{y_1^2(k) + \mathbf{u}^T(k)\mathbf{R}\mathbf{u}(k)\}\,, \tag{14}$$

where y_1 is the head displacement output. The design parameter in the DLQR design is the control action weight matrix $\mathbf{R}$, which can be tuned to obtain desired system responses.

3.1.3 Simulation results

As briefly described in the previous section, the choice of the process noise weights was based on the PSD of the open-loop PZT sensor output. The remaining parameters, the measurement noise variance V_2 and the control action weight matrix $\mathbf{R}$, can be set/tuned to obtain a desired damped system. A Simulink model was used to tune these parameters, which also allowed us to test the effects of the computational delay and the noise induced by the single-precision floating point arithmetic on the damping controller. Figs. 8 and 9 show the simulation results of the damped transfer functions from the VCM and PZT actuator to the head displacement, respectively.

3.2 Track-Following Controller Design

Once the inner-loop damping control design is completed, the outer-loop track-following controller can be designed based on the damped actuator models. There are several popular techniques for designing dual-stage track-following controllers. In this paper, a simple sensitivity transfer functions decoupling method, which is also referred as the decoupled master-slave, or the series compensator method, has been used [6], [8].

Fig. 10 shows a block diagram for dual-stage track-following controller design using this method. In the figure, r represents the track runout; G_{VCM} and G_{MA} are the (damped) VCM and PZT actuator models, respectively. K_{VCM} and K_{MA} are the VCM and PZT-actuator loop controllers, respectively. The displacement of the PZT actuator relative to that of the VCM, $RPESS$, is estimated by multiplying the PZT control input by the DC gain of the PZT actuator, g_{PZT}. It can be shown that the total closed-loop sensitivity function of the dual-stage servo system in Fig. 10 is approximately equal to the series of the sensitivity functions corresponding to the VCM and PZT-actuator loops. Thus, the design of the dual-stage servo controller can be decoupled. First, the VCM loop compensator can be designed independently. Then, the PZT loop compensator is designed to expand the bandwidth of the overall control system [6].

The VCM loop compensator, $K_{VCM}(s)$, was designed to be a lead-lag compensator. The VCM loop gain cross-over frequency was chosen to be 800 Hz. The PZT actuator loop compensator, $K_{MA}(s)$, was designed to be a lag compensator. The PZT actuator loop gain cross-over frequency was chosen to be 2500 Hz. Notch filters are not used because the resonance modes are adequately damped by the damping control loop.

The Bode plot of the overall open-loop transfer function with the track-following controller from r to y_1 (damping control loop closed) is shown in Fig. 11. The gain cross over frequency, the gain margin and the phase margin of the dual-stage control system are $2425Hz$, $3.4dB$ and 37°, respectively.

4 Experimental Results

First, the inner-loop damping controller was tested. Figs. 12 and 13 compare the frequency responses of the damped system to those of the open-loop system, from the VCM and PZT actuator to the head displacement, respectively. Both the butterfly mode and the suspension sway mode are attenuated by damping control. Fig. 14 shows the PSD of the head lateral motion measured by the LDV and the HP digital analyzer when damping control is and is not applied. As shown in the figure, the air turbulence excited high-frequency structural vibrations are attenuated by damping control. The RMS value of the PSD from 2 kHz to 14 kHz is reduced by 35% when damping control is applied.

Second, the outer-loop track-following controller with the inner-loop damping control was tested. Fig. 15 shows the FFT of the head-off track motion with track-following control. The solid line is the result with combined track-following and vibration damping control. The dashed line is the result of traditional decoupled design without the inner damping control loop. With damping control, the high-frequency vibrations can be greatly attenuated. The track-following controller with damping control also has a larger disturbance attenuation in the low-frequency range because of the increased bandwidth. The standard deviation of the position error of the damping control design is 4.8 nm, while that of the traditional notch filter design is 6.1 nm.

5 Conclusion

A track-following controller design with active vibration damping has been proposed for a PZT-actuated suspension dual-stage servo system. A state feedback inner-loop damping controller was designed to actively damp multiple resonances modes using one PZT elements on a PZT-actuated suspension as a vibration sensor. A high bandwidth outer-loop track-following controller was designed based on the damped dual-stage actuator model. Experimental results confirm the effectiveness of the proposed control scheme in suppressing structural vibrations and enhancing the overall performance of the servo system.

The use of one PZT element as a vibration sensor provides a simple and effective solution to active vibration control of the PZT-actuated suspension dual-stage servo system. However, there are also some limitations to this scheme since the PZT element was not originally designed to be a sensor. It cannot sense some off-track modes, while it picks up some non-off-track modes. This makes the vibration controller complicated. The damping controller design can be simplified if an optimally designed vibration sensor is available.

References

[1] R.B. Evans, J.S. Griesbach, and W.C. Messner "Piezoelectric microactuator for dual-stage control", *IEEE Transaction on Magnetics,* pp 977-81, Vol. 35, March, 1999

[2] F.-Y. Huang, T. Semba, W. Imaino, and F. Lee, "Active damping in HDD actuator" *IEEE Trans. Magn.*, vol. 37, pp. 847–849, Mar. 2001.

[3] M. Kobayashi, S. Nakagawa, and S. Nakamura "A phase-stabilzed servo controller for dual-stage actuators in hard disk drives", *IEEE Transaction on Magnetics,* March, 2003

[4] Y. Li, R. Horowitz, and R. Evans "Vibration Control of a PZT Actuated Suspension Dual-Stage Servo System using a PZT Sensor", *IEEE Transaction on Magnetics,* March, 2003

[5] K. J. Åström and B. Wittenmark. *Computer Controlled System.* Prentice-Hall, Inc, 3rd edition, 1997.

[6] Y. Li and R. Horowitz, "Design and Testing of Track-Following Controllers for Dual-Stage Servo Systems with PZT Actuated Suspensions", *Microsystem Technologies,* Vol. 8, Issue 2-3, May 2002.

[7] D.J. Ewins, *Modal Testing: Theory, Pratice and Application,* 2nd edition, Research Studies Press Ltd., 2000

[8] K. Mori, T. Munemoto, H. Otsuki, Y. Yamaguchi, and K. Akagi, "A dual-stage magnetic disk drive actuator using a piezoelectric device for a high track density," *IEEE Transactions on Magnetics*, vol. 27, no. 6, pp. 5298–5300, November 1991.

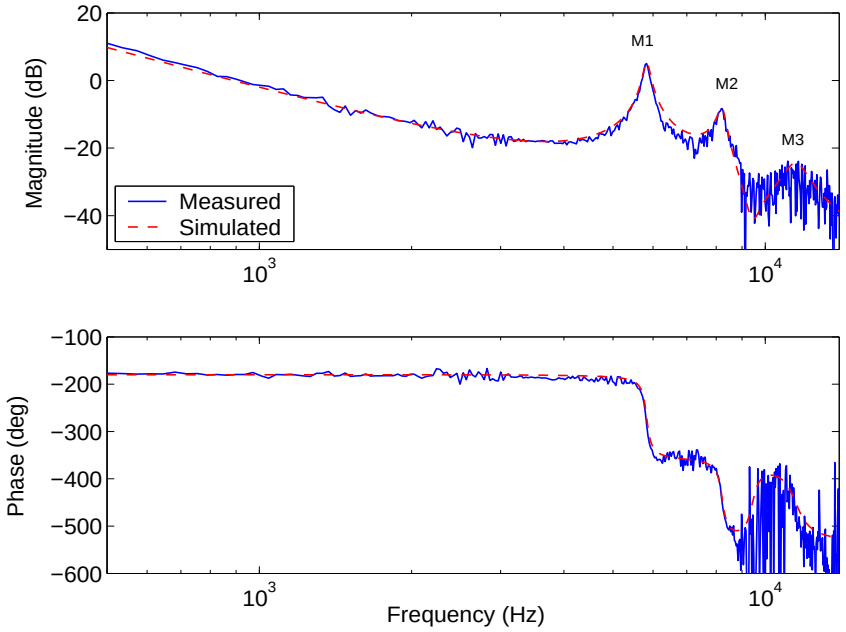

Figure 1: Frequency response from VCM input to head displacement.

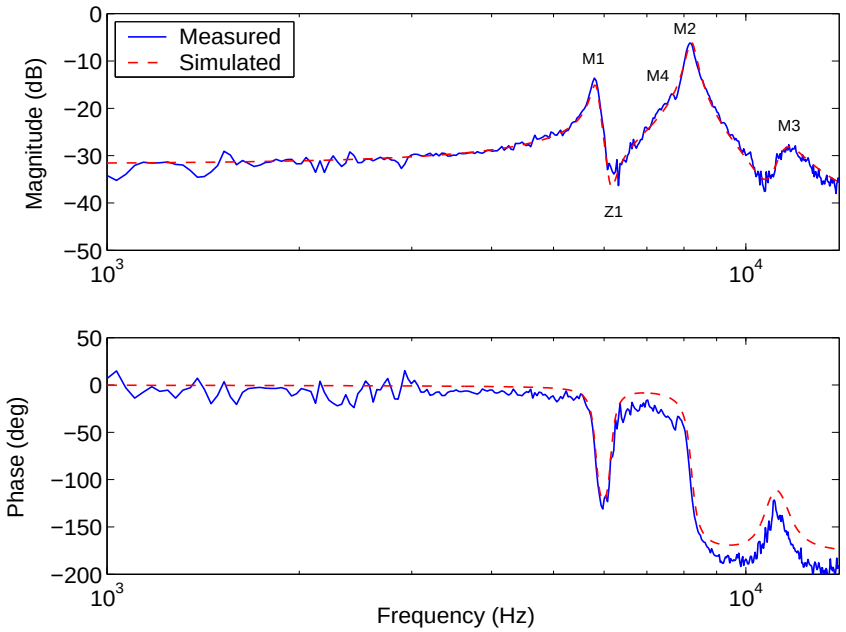

Figure 2: Frequency response from PZT actuator input to head displacement.

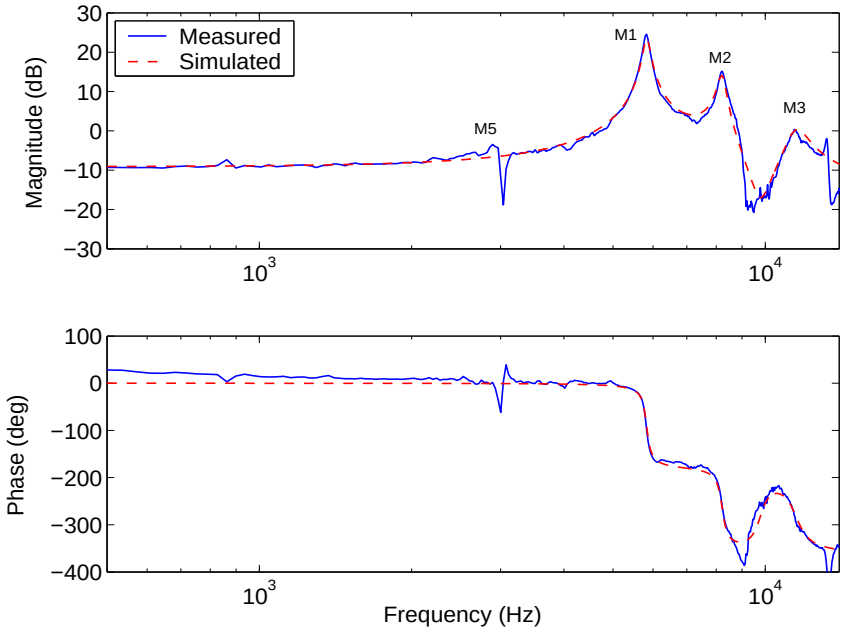

Figure 3: Frequency response from VCM input to PZT sensor output.

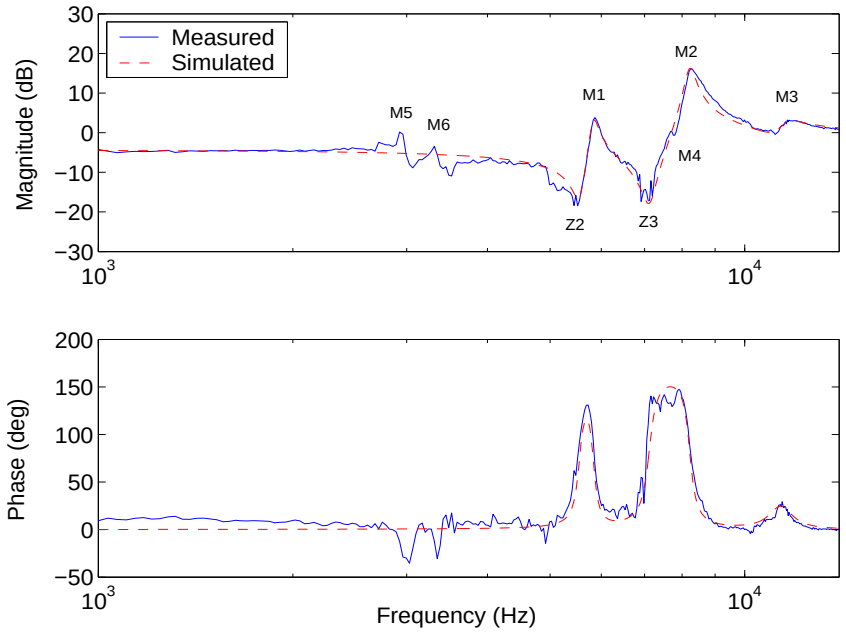

Figure 4: Frequency response from PZT actuator input to PZT sensor output.

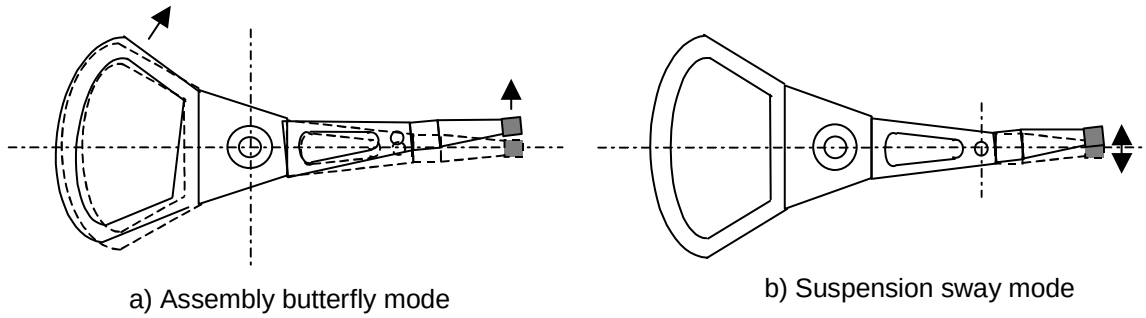

Figure 5: Illustration of modes shape of assembly butterfly mode and suspension sway mode.

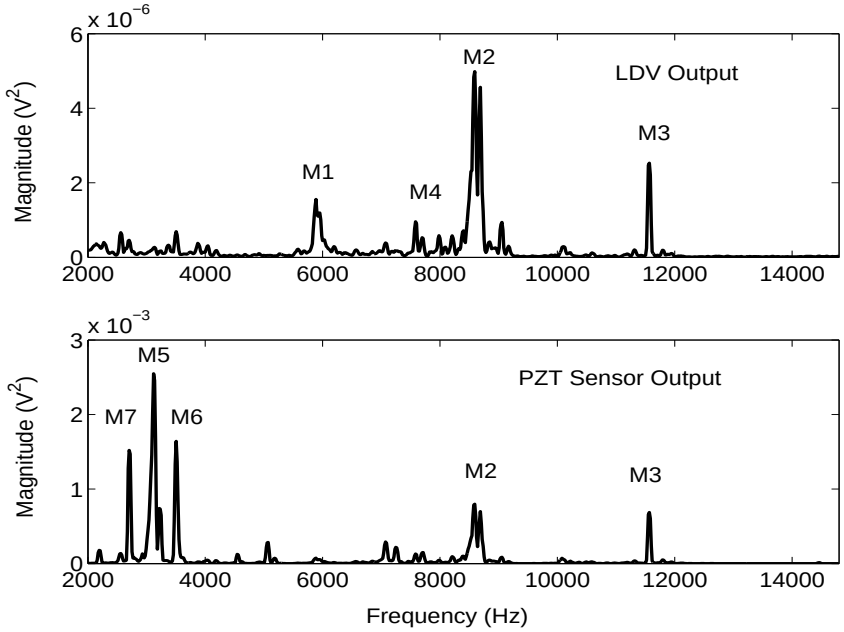

Figure 6: PSDs of the head off-track motion and the PZT sensor output due to airflow excited vibrations.

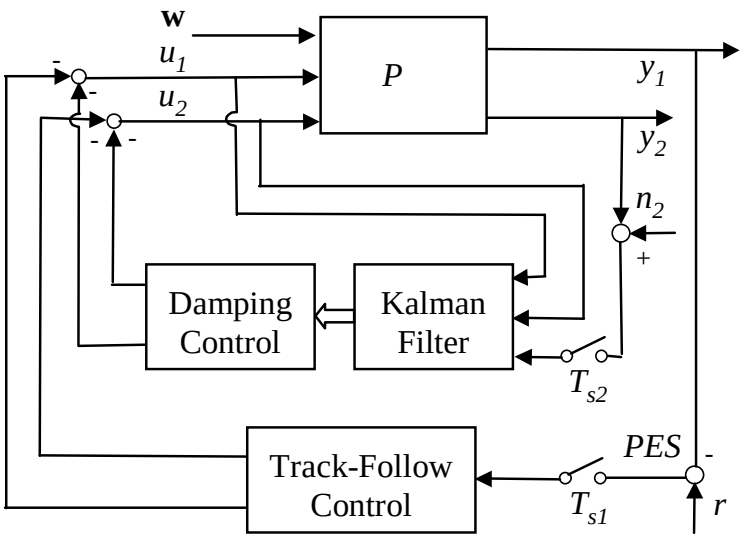

Figure 7: A block diagram of the control system.

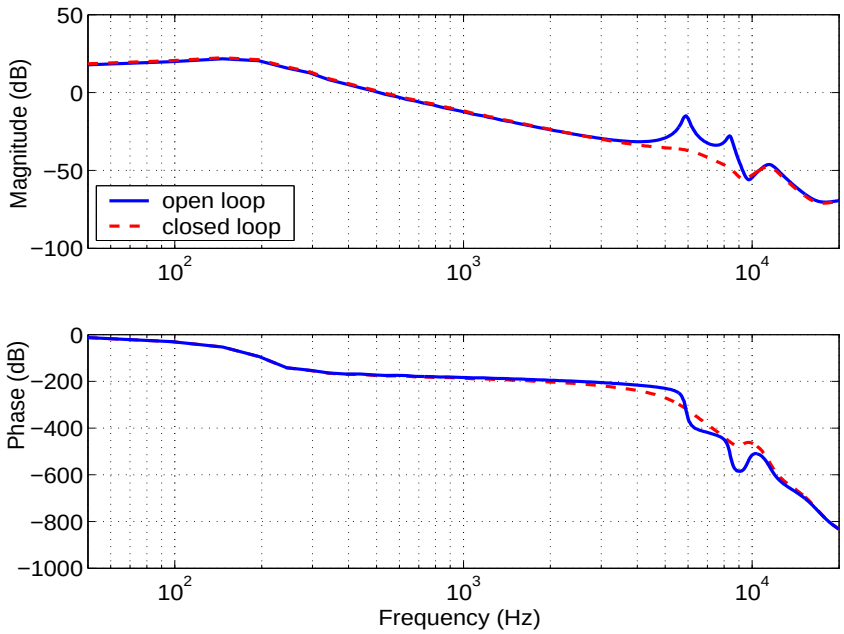

Figure 8: Simulated frequency response from the VCM to the head displacement.

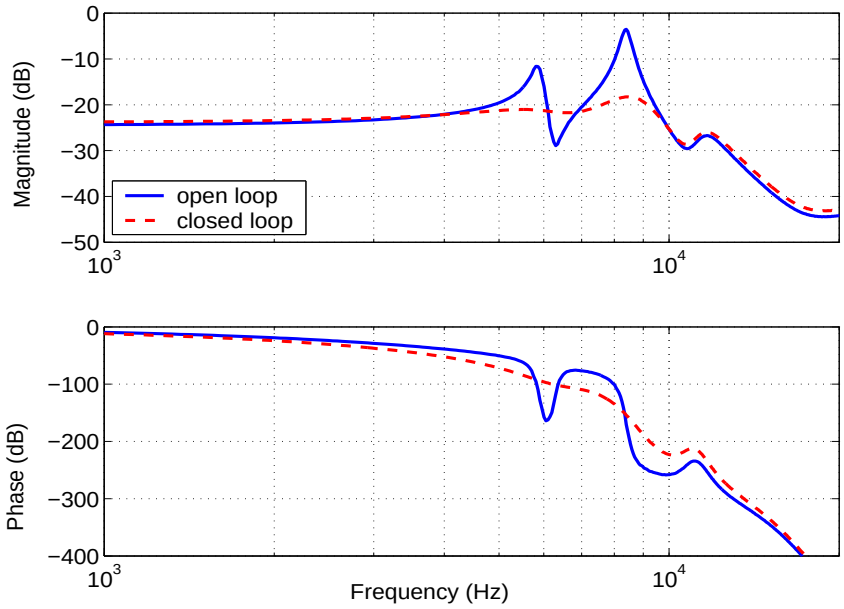

Figure 9: Simulated frequency response from the PZT actuator to the head displacement.

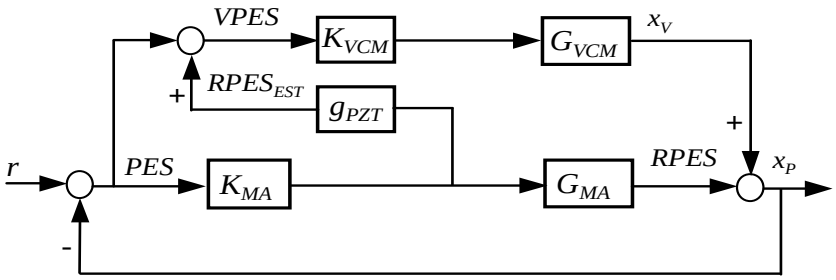

Figure 10: Block diagram of the track-following controller design

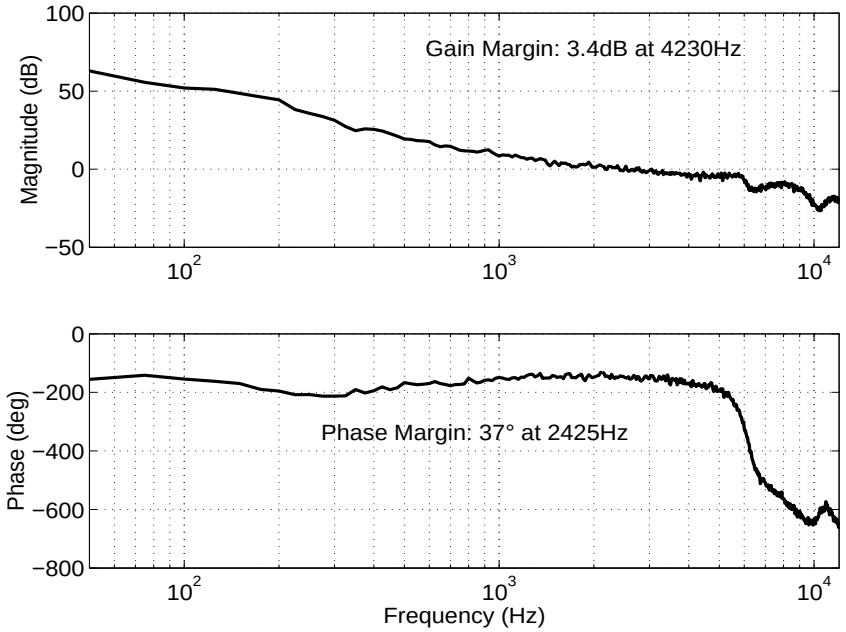

Figure 11: Open-loop Bode plots

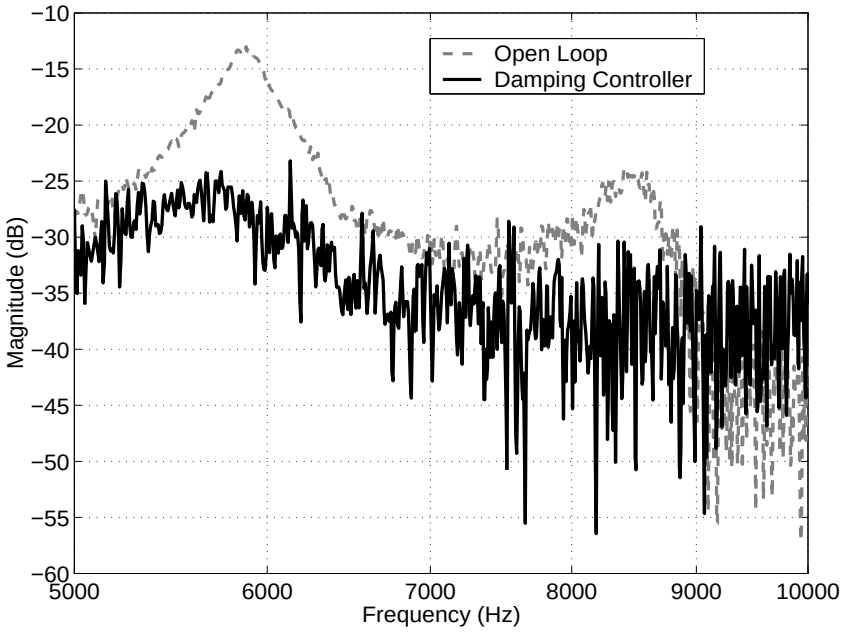

Figure 12: Measured frequency response from the VCM to the head displacement.

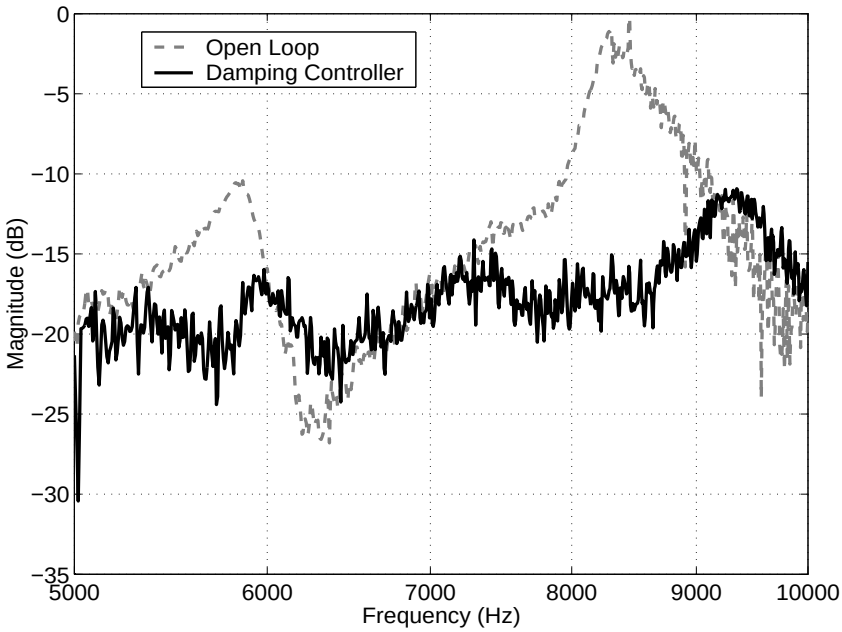

Figure 13: Measured frequency response from the PZT actuator to the head displacement.

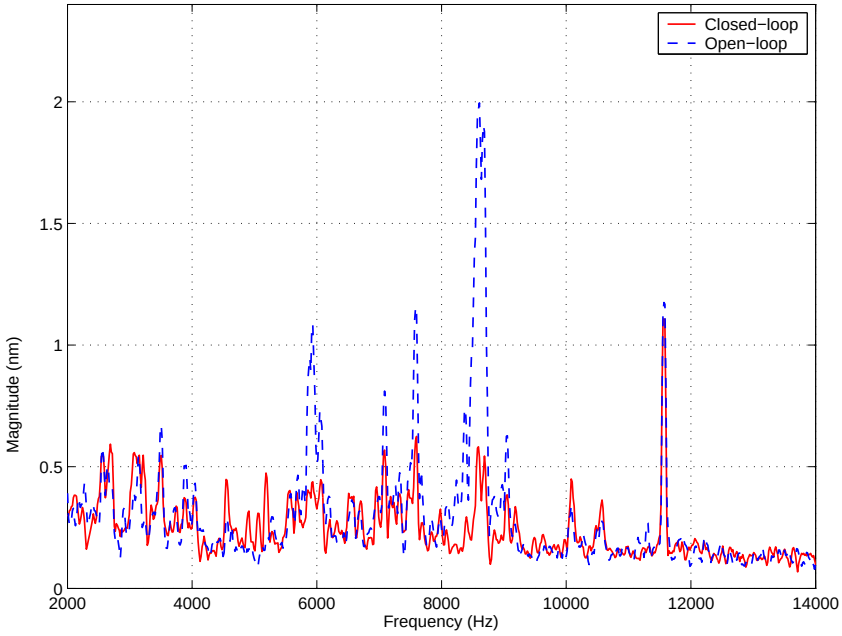

Figure 14: Measured PSD of head off-track motion with damping control.

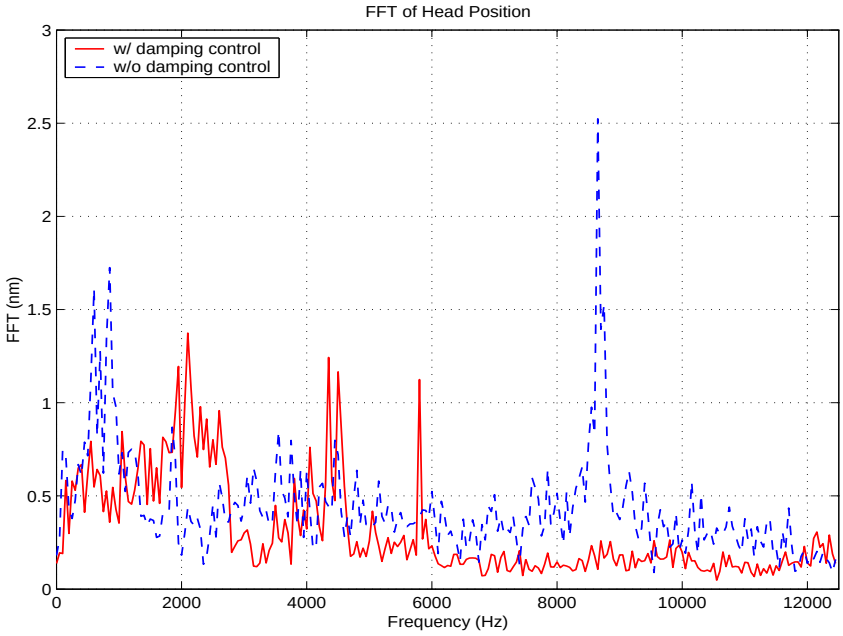

Figure 15: FFT of the head off-track motion with both damping and track-following control.